# REPORT DOCUMENTATION PAGE

AFRL-SR-AR-TR-05-

0511



| 1. REPORT DATE *(DD-MM-YYYY)* | 2. REPORT TYPE | 3. DATES COVERED *(From - To)* |
|---|---|---|
| 30-11-2005 | Final Technical Report | 15-05-2002 - 31-08-2005 |

**4. TITLE AND SUBTITLE**

Non-Thermal, Non-Ionizing Interaction of High-Intensity Electromagnetic Fields with Small-Scale Electronic and Biological Systems

**5a. CONTRACT NUMBER**

**5b. GRANT NUMBER**
F49620-02-1-0257

**5c. PROGRAM ELEMENT NUMBER**

**6. AUTHOR(S)**

J. Scott Tyo & Deborah G. Evans

**5d. PROJECT NUMBER**

**5e. TASK NUMBER**

**5f. WORK UNIT NUMBER**

**7. PERFORMING ORGANIZATION NAME(S) AND ADDRESS(ES)**

University of New Mexico
1 Scholes Hall
Albuquerque, NM 87131

**8. PERFORMING ORGANIZATION REPORT NUMBER**

**9. SPONSORING / MONITORING AGENCY NAME(S) AND ADDRESS(ES)**

AFOSR/NE
801 N. Randolph St, room 732
Arlington, VA 22203

**10. SPONSOR/MONITOR'S ACRONYM(S)**

AFOSR/NE

**11. SPONSOR/MONITOR'S REPORT NUMBER(S)**

**12. DISTRIBUTION / AVAILABILITY STATEMENT**

DISTRIBUTION STATEMENT A
Approved for Public Release
Distribution Unlimited

Unlimited

**13. SUPPLEMENTARY NOTES**

**14. ABSTRACT**

This portion of the State of New Mexico's FY2002 DEPSCoR improved the capabilities of the University of New Mexico to participate in electromagnetic effects testing and analysis on electrical and biological systems through the development of a short-pulse, high-field intensity test structures in the Electrical and Computer Engineering Department. Our program focused on two interrelated areas: 1) the design, construction, and testing of a tunable pulser system, and 2) development of physical chemistry models that can be used to predict and explain phenomenology that we observe in these test.

**15. SUBJECT TERMS**

Electromagnetics, Pulsed Power, High Power Microwaves

| 16. SECURITY CLASSIFICATION OF: | | | 17. LIMITATION OF ABSTRACT | 18. NUMBER OF PAGES | 19a. NAME OF RESPONSIBLE PERSON |
|---|---|---|---|---|---|
| a. REPORT | b. ABSTRACT | c. THIS PAGE | | | J. Scott Tyo |
| U | U | U | Unlimited | 30 | 19b. TELEPHONE NUMBER *(include area code)* 505-277-1412 |

Final Technical Report
May 15, 2002 – August 31, 2005

# Non-Thermal, Non-Ionizing Interaction of High-Intensity Electromagnetic Fields with Small-Scale Electronic and Biological Systems

Award Number: F49620-02-1-0257

Submitted to:
Dr. Robert J. Barker
AFOSR/NE
801 N. Randolph St, Room 732
Arlington, VA 22203

PI: J. Scott Tyo
Electrical and Computer Engineering Department
University of New Mexico
Albuquerque, NM 87131-1356 USA
tyo@ieee.org

Co-PI: Deborah G. Evans
Chemistry Department
University of New Mexico
debi@unm.edu

# 1 Introduction

## 1.1 Objectives

This portion of the State of New Mexico's FY2002 DEPSCoR improved the capabilities of the University of New Mexico to participate in electromagnetic effects testing and analysis on electrical and biological systems through the development of a short-pulse, high-field intensity test structures in the Electrical and Computer Engineering Department. Our program focused on two interrelated areas: 1) the design, construction, and testing of a tunable pulser system, and 2) development of physical chemistry models that can be used to predict and explain phenomenology that we observe in these test.

## 1.2 Technical Background

There is a significant interest in wideband (WB) and ultra wideband (UWB) electromagnetic sources for a variety of applications including UWB communications, UWB and ground penetrating RADAR, and electronic warfare [1, 2, 3]. The development of sources and applications for UWB technology also brings out the need for systems that can support electromagnetic interference (EMI) and electromagnetic compatibility (EMC) testing with WB/UWB waveforms. Traditionally, effects testing has been preceded by the development of sources for particular applications. Invariably, the sources designed for particular scenarios are relatively inflexible in the choice of parameters of operation, such as center frequency, pulse bandwidth, pulse repetition rate (PRR), pulse amplitude, and burst pattern. A source thats is adjustable with regard to the above mentioned parameters would be of great benefit to the study of the interaction of transient electromagnetic fields with small scale electrical [4] and biological [5] systems.

Because of this lack of agility on the part of most WB sources, and in order to test a large region of the parameter space, we have designed a tunable source topology to produce fields for effects testing that will range up to 30 kV/cm. Our primary interest is for WB/UWB waveforms with center frequencies ranging from several hundred MHz to a few GHz and bandwidths on the order of 10% – 200 %. In this report, we present the design and characterization of a source to address this need. We also discuss biological modeling that has been done in order to assess electromagnetic coupling to these systems.

# 2 Blumlein Operation

## 2.1 Ideal Blumlein

The Blumlein is a type of vector inversion pulse generator that takes advantage of multiple transmission lines to generate a waveform of interest. A circuit model of an ideal Blumlein is shown in fig. 2. Briefly, the Blumlein operates by differentially charging two transmission lines of characteristic impedance $Z_0/2$ in parallel to a voltage $V_0$. At time $t = 0$, switch in fig. 2 closes, launching waves of $\pm V_0/2$ on the two lines. The short at the end of one line and the open at the end of the other line cause opposite-signed reflection coefficients, and the resulting pulse output into the load resistance of $Z_0$ is a pulse of amplitude $V_0$ for a time equal to the two way transit

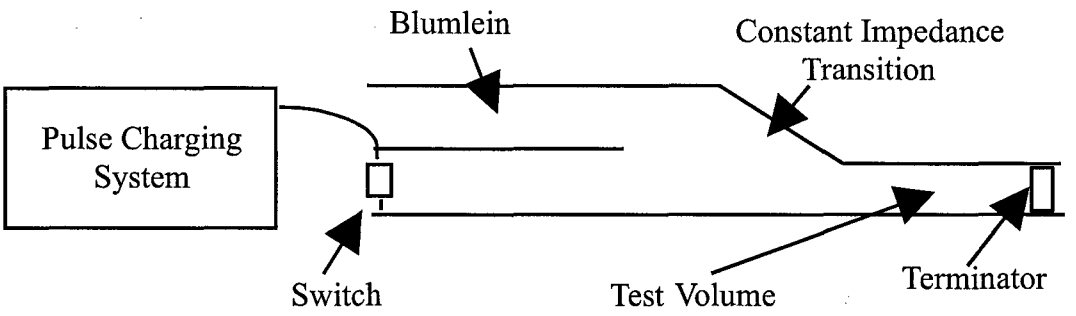


Figure 1: The general experimental topology is to have a parallel plate Blumlein with the movable center electrode pulse charged. The output is a parallel plate Blumlein with a testing volume and a terminating load.

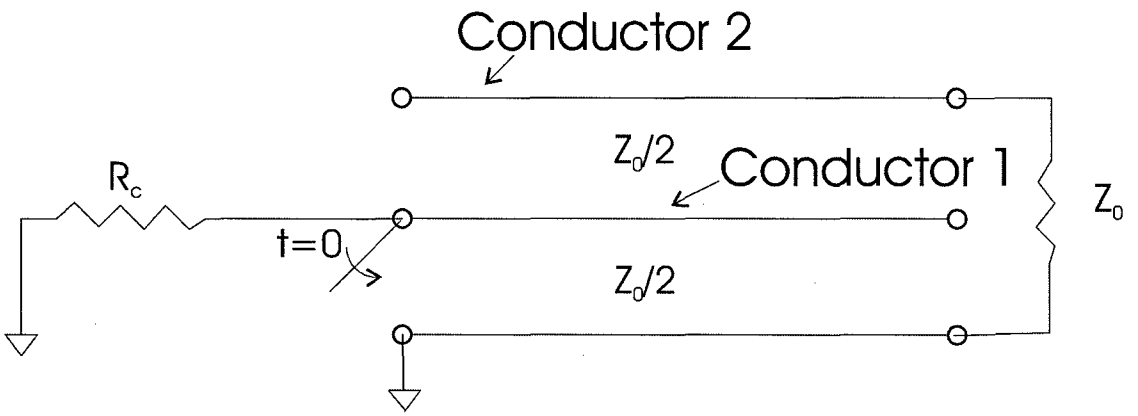


Figure 2: Circuit model of the ideal Blumlein. $R_c$ is a large charge resistor.

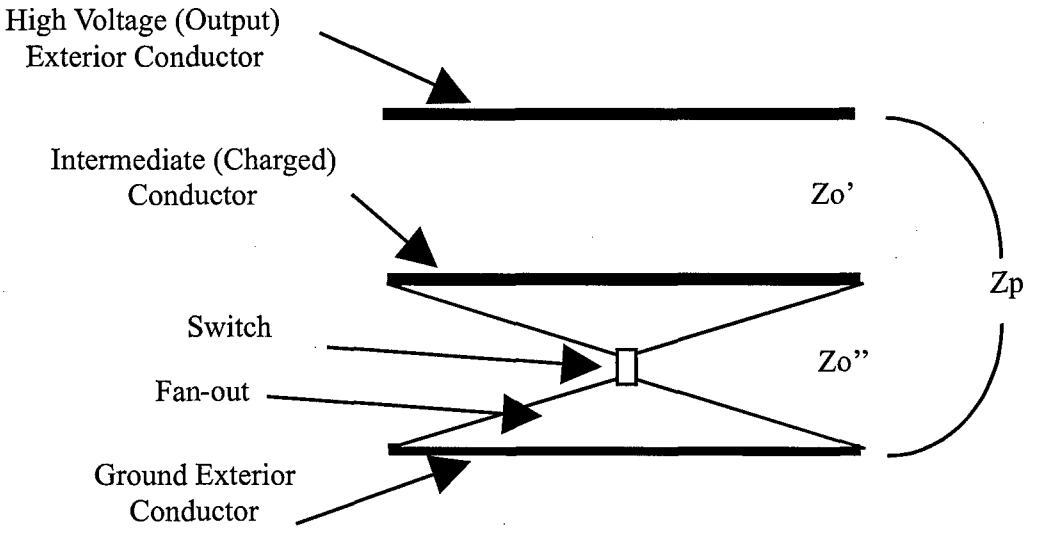


Figure 3: A parallel plate Blumlein suffers from parasitic capacitances (and impedances) between the topmost and bottommost electrodes. These parasitics degrade the performance of the ideal Blumlein, and must be taken into account in the circuit diagram in fig. 2.

time on the pulse forming network (PFN). Multiple Blumleins can be "stacked" to realize voltage multiplication in a Marx generator-like configuration [6].

In an ideal Blumlein, there is no coupling between the two transmission lines other than through currents flowing on the common electrode. In practice, the two lines are made either from a coaxial geometry or in a parallel plate configuration. In the coaxial configuration, the approximation of electromagnetically uncoupled lines is quite good. However, in a parallel plate configuration, there can be significant coupling of the two transmission lines through electric fields instead of currents [7]. This coupling can be included as a parasitic impedance as depicted in fig. 3.

The parasitic impedance terms that result from this coupling degrade the ideal performance of the Blumlein. Specifically, the output pulse amplitude is reduced from the ideal $V_0$ charge voltage and the waveform has some ringing [7]. In addition, the benefits of stacking Blumleins can be reduced due to these parasitic coupling terms. The parasitic impedance can be controlled by modifying the geometry as presented below [7].

In addition to the parasitic impedance terms, alteration of the two line impedances in fig. 2 from their ideal value of $Z_0/2$ can affect the output waveform. We capitalize on this property in designing our frequency agile source.

## 2.2 Source Design

Referring to fig. 3, our source is composed of two exterior transmission line plates that ultimately form the output section of the Blumlein. An intermediate transmission line plate is placed be-

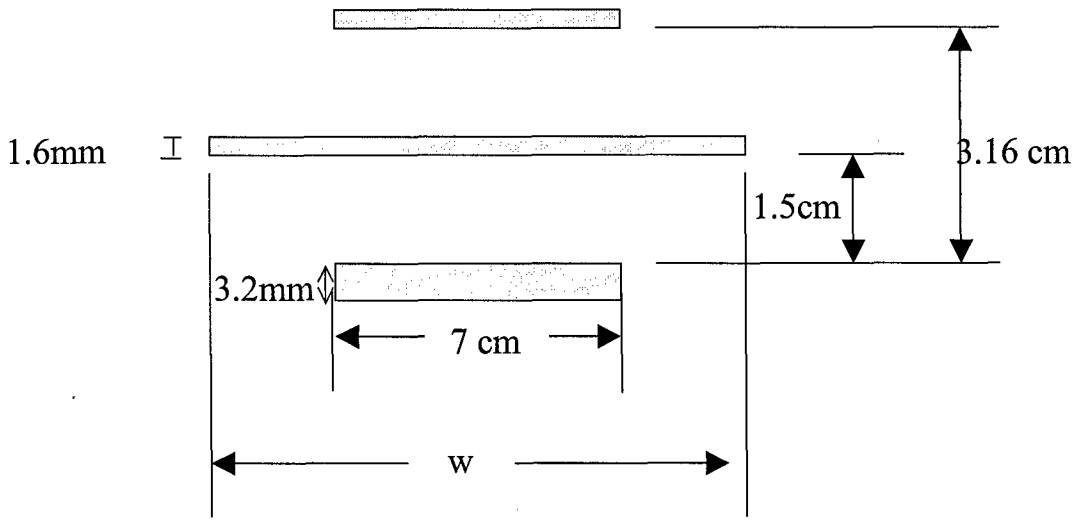


Figure 4: Schematic of the cross section fed into the Electro simulation. The top two plates were taken as 1.6 mm (1/16") thick and the bottom plate was 3.2 mm (1/8") thick. The length was taken to be 30 cm (1 ns transit time).

tween the two exterior plates and charged to $V_c$. A switch (ultimately a self-break Hydrogen switch) closes to electrically connect the intermediate plate to the bottom plate, which in this case is grounded.

In our application, the Blumlein output impedance (the impedance between the exterior conductors with no intermediate conductor present) is selected to be approximately 100 Ω. It has been shown that the output to charge voltage ratio ($V_0/V_c$) of a Blumlein is related to the ratio of the intermediate plate width to the exterior conductor plate widths because of the reduction in the parasitic capacitances in the Blumlein [7]. Experimental investigations have indicated that although increasing the intermediate conductor plate width does in fact increase the ratio Vo/Vc, the increased plate width may increase the rise time to maximum output voltage as compared to an intermediate plate equal in width to the two exterior conductors. For this application, an intermediate plate width equal to the exterior conductors was selected and compared with the performance of a switch with a center conductor 2.5 times wider than the outer conductors. The results are presented below.

# 3 System Modeling

## 3.1 Determination of Electromagnetic Parameters

The Blumlein impedances were evaluated using the Electro software package [8]. Electro is an electrostatics code that computes solutions to the Poisson equation, allowing the capacitance of a finite-length transmission line structure to be determined. A schematic of an Electro Blumlein model is shown in fig. 4. The dimensions of the Blumlein were selected to maintain the desired impedance as well as to accommodate the 1.5 cm tall gas switch that will ultimately be incorpo-

Table 1: Center electrode configurations tested in this paper. Dimensions are all relative to fig. 3. Negative offsets are taken towards the bottom conductor.

| # | width (cm) | offset (mm) |
|---|---|---|
| 0 | 21 | 0 |
| 1 | 7 | 0 |
| 2 | 7 | -3.8 |
| 3 | 7 | -7.6 |
| 4 | 7 | -12.4 |
| 5 | 7 | +12.4 |

rated into the Blumlein. The switch is described in section 5.1. For the Electro analysis, the top and intermediate conductors were assigned as conductors 1 and 2 respectively and the bottom conductor is assigned as ground. We are designing our system to work in the frequency range from a few hundreds of MHz to a few GHz, so we chose a Blumlein length of 1 ns ($\ell = 30\,\text{cm}$), which gives a center frequency for an ideal Blumlein output of 500 MHz.

The Electro simulation allows us to compute the capacitance matrix **C** of the multi conductor transmission line structure that forms the Blumlein PFN. The capacitance matrix is determined by holding conductor 1 at a fixed potential and holding the conductor 2 to ground. The total charge on conductor 1 is used to calculate $C_{11}$, and the total charge accumulated on conductor 2 is used to calculate $C_{12}$. The process is then repeated with conductor 2 held at a fixed potential and conductor 1 held at ground to compute $C_{22}$ and $C_{21}$. The capacitance matrix of configuration 1 from table 1 as depicted in fig. 4 is (in units of Farads) is

$$\mathbf{C} = \begin{bmatrix} 1.73 \times 10^{-11} & 1.47 \times 10^{-11} \\ 1.47 \times 10^{-11} & 2.96 \times 10^{-11} \end{bmatrix} \tag{1}$$

We can use these capacitances to compute the relevant transmission line impedances as [9]

$$Z_0' = \frac{\ell/c}{C_{21}} = 68\Omega, \tag{2}$$

$$Z_0'' = \frac{\ell/c}{C_{22} - C_{21}} = 67\Omega, \tag{3}$$

$$Z_p = \frac{\ell/c}{C_{11} - C_{12}} = 384\Omega, \tag{4}$$

where $\ell/c$ is the transit time of the PFN and the impedances are defined in fig. 3. The impedances $Z_0'$, $Z_0''$, and $Z_p$ are defined in fig. 3.

Table 1 presents the configurations that we tested in this paper. The various configurations had either a narrow or wide center conductor, and had the center conductor offset towards the top (positive offsets) or bottom (negative offsets) electrode.

Fig. 5 shows the cross section and the Electro predicted equipotential lines for configuration 5. The cross sections for the other tested configurations are similar, with the center conductor

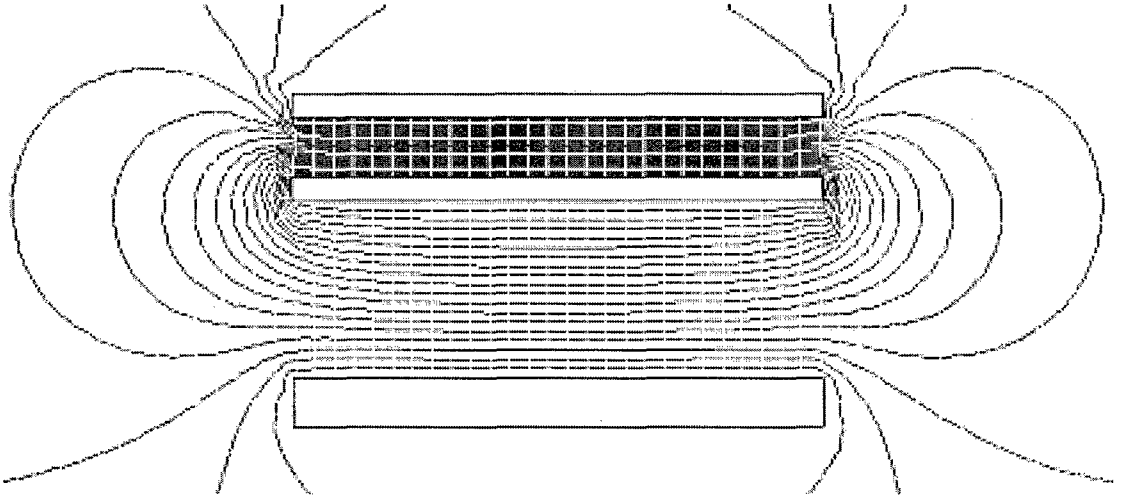

Figure 5: Equipotential contours for the transmission line cross section corresponding to configuration 5 in table 1. The field enhancement in the upper region causes a reduction in $Z_0'$ and a corresponding increase in $Z_0''$.

offset towards one of the outer electrodes. Note that there is field enhancement in the upper region, as expected, causing a decrease in the impedance of the upper transmission line and an increase in the impedance of the lower line. This unbalanced impedance causes the Blumlein to deviate from its ideal performance, as discussed in section 3.2 below.

### 3.2 Circuit Modeling

Once the impedances $Z_0'$, $Z_0''$, and $Z_p$ are known, the performance of various Blumlein conductor configurations can be predicted using a circuit simulator such as Pspice [10]. The PSpice circuit diagram that we are using is shown in fig. 6. The impedance of the exterior conductors without the intermediate conductor was calculated using Electro to be 107Ω. Fig. 7 shows the response predicted by PSpice into the load in fig. 6. For configuration 1, there is a slight amount of ringing due to the parasitic capacitance discussed above. As the center conductor is offset towards the bottom conductor, this ringing is enhanced. By moving the center conductor towards the top conductor (configuration 5) a decaying waveform is obtained. Since the PSpice model does not include any losses (radiation or resistance), the waveforms are step-like. The inclusion of losses would make the responses more sinusoidal in nature with increased damping.

## 4 Low Voltage System Tests

### 4.1 Adjusting Bandwidth

In order to test the utility of the proposed architecture, we have performed a number of tests using a low voltage system. For our preliminary experiments reported here, the center conductor

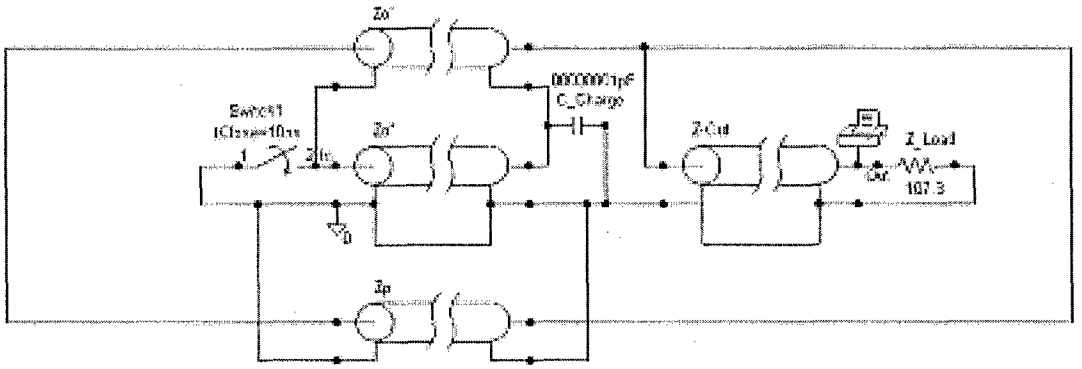


Figure 6: PSpice circuit diagram showing the two Blumlein impedances, the parasitic impedance, the output transmission line, and the matched load. Note that the load is the only source of loss in this model, which cannot account for line and radiation losses.

was DC charged to 130 V using an Ultravolt 1C24-P125 DC-DC converter, and the switch used was a 2N2222 triggered transistor. Output voltage measurements were made with a capacitive voltage probe situated on the bottom electrode. The configurations listed in table 1 were realized by swapping out center conductors of different sizes and at different locations.

Fig. 8 shows the measured output voltage for configurations 0 and 1 in the low voltage test fixture. The data in this figure demonstrates the benefit of using a wider center conductor. Note from the figure that the Blumlein with the wide center conductor has an output voltage which is almost 100% of the charge voltage. In contrast, the Blumlein with the narrow center conductor has an output voltage of approximately 83% of the charge voltage. This is in agreement with earlier simulations [7]. However, the rise time penalty measured earlier is not apparent at these rise time scales.

Fig. 9 shows the measured responses for configurations 1 – 5 in table 1. Note that the output waveform varies between an exponential decay and an under-damped ringing waveform based only on the vertical location of the Blumlein center conductor. The trends predicted by the Pspice simulations shown in fig. 7 are realized in the measured data, and the agreement is best for configuration 5. Both the polarity of the ringing and the approximate Q of the circuit is predicted by the model. Fig. 10 shows the energy spectral densities (ESDs) of the waveforms in fig. 9. The ESDs in fig. 10 clearly show that the spectral content of the waveform is changing. Fig. 12 shows the cumulative energy distribution in for the ESDs in fig. 10. The waveform for configuration 5 is concentrated at low frequencies due to the longer positive pulse. Configurations 3 and 4 show an increase of the concentration of energy around the first and second harmonics of the ringing relative to configuration 1. Note that there is a slight shift of the frequency spectra between configurations 1 and 3, which is probably due to the larger positive ring in the latter case, which makes the apparent width of the main pulse smaller (higher frequency).

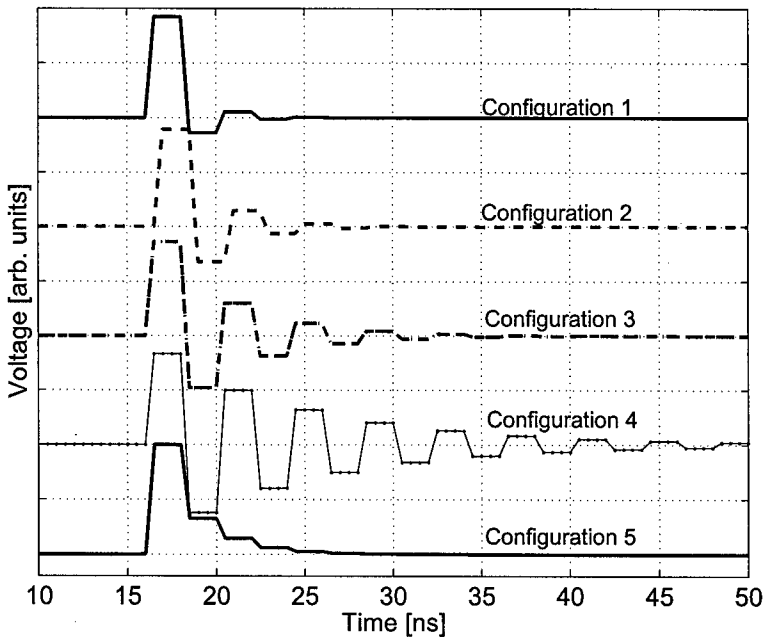


Figure 7: PSpice predicted responses for configurations 1 – 5 in table 1.

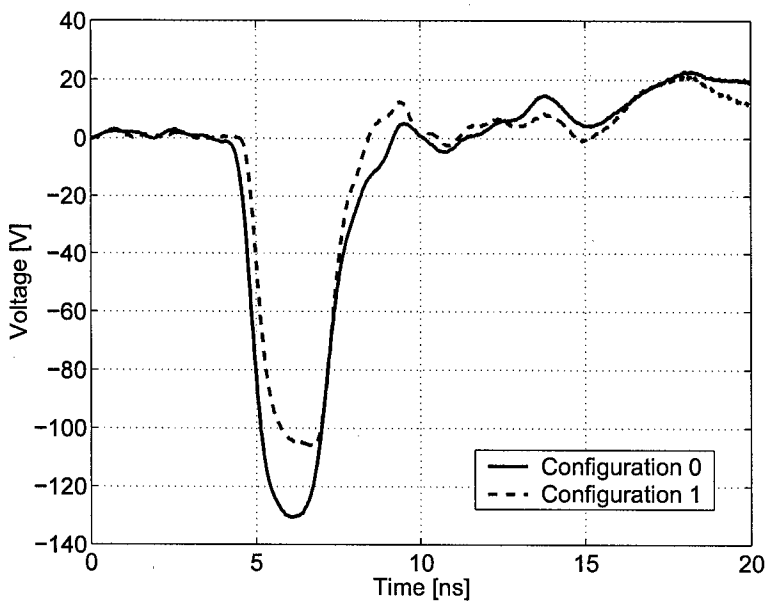


Figure 8: Measured output voltage for configurations 0 and 1 in table 1. The wider center conductor used in configuration 0 results in greater Blumlein efficiency.

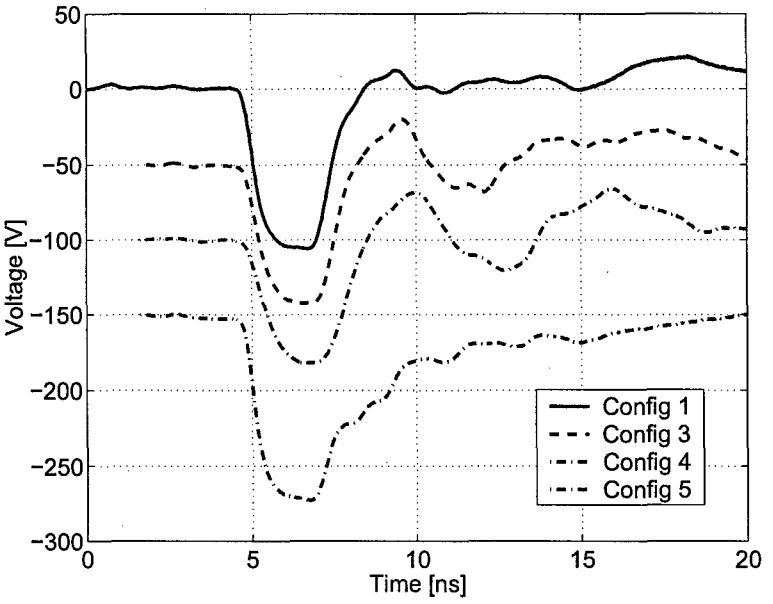


Figure 9: Low voltage test cell responses for configurations 1 – 5 in table 1.

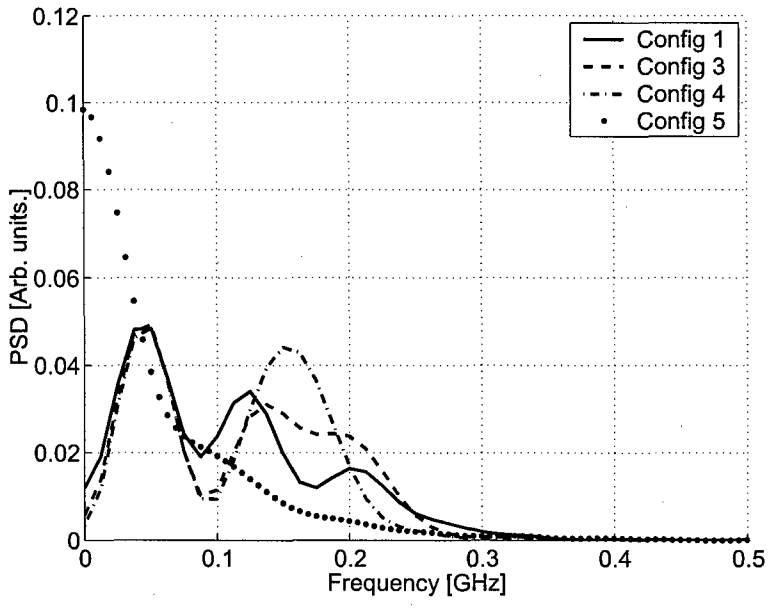


Figure 10: Normalized energy spectral densities (ESDs) of the waveforms in fig. 9 in the low voltage tests. The ESDs are normalized to the total energy in each waveform.

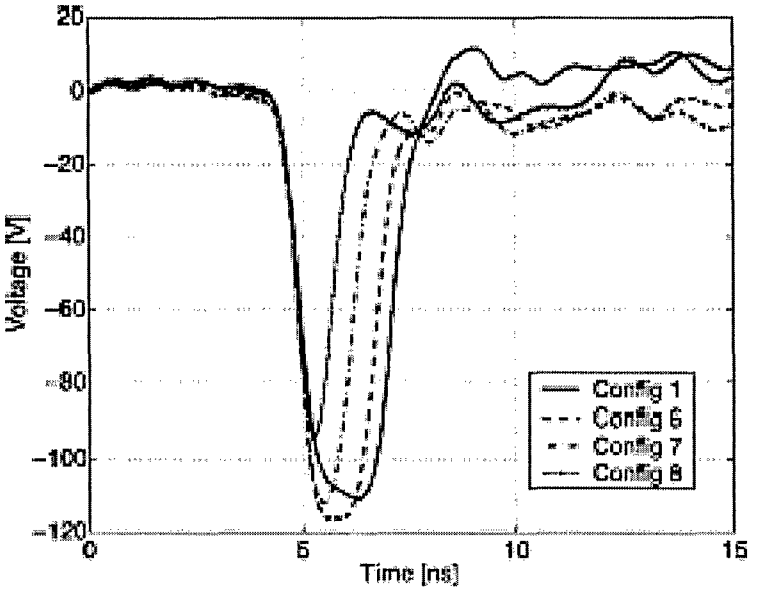


Figure 11: Variable pulsewidth obtained by retracting the center conductor on a low-voltage prototype as directed in fig. 14 [11].

Table 2: Configurations tested by retracting the center conductor as shown in fig. 13.

| # | $\ell_i$ (cm) | $\ell_o$ (cm) |
|---|---|---|
| 1 | 30 | 0 |
| 6 | 22.5 | 7.5 |
| 7 | 15 | 15 |
| 8 | 7.5 | 22.5 |

## 4.2 Adjusting the Center Frequency

We stated above that our goal is to design a pulser with tunable bandwidth *and* center frequency. The results presented above demonstrate that bandwidth can be tuned by offsetting the center conductor of the Blumlein structure. In order to tune the center frequency, the length of the energy storage section $\ell$ must be changed. As a first step, we performed a series of experiments where we simply slid the center conductor out of the Blumlein. In this case, the total length of the center conductor remained fixed, but the portion between the center conductors was reduced as shown in fig. 13. This is not an ideal solution, as there is still coupling between the extracted portion of the center conductor and the outer conductors.

Table 2 lists the configurations tested in this experiment. The center electrode width was the same for all of these test (7 cm). The measured response in each case is shown in fig. 14. Due to the physical constraints of our test fixture, we were not able to retract the center plate in

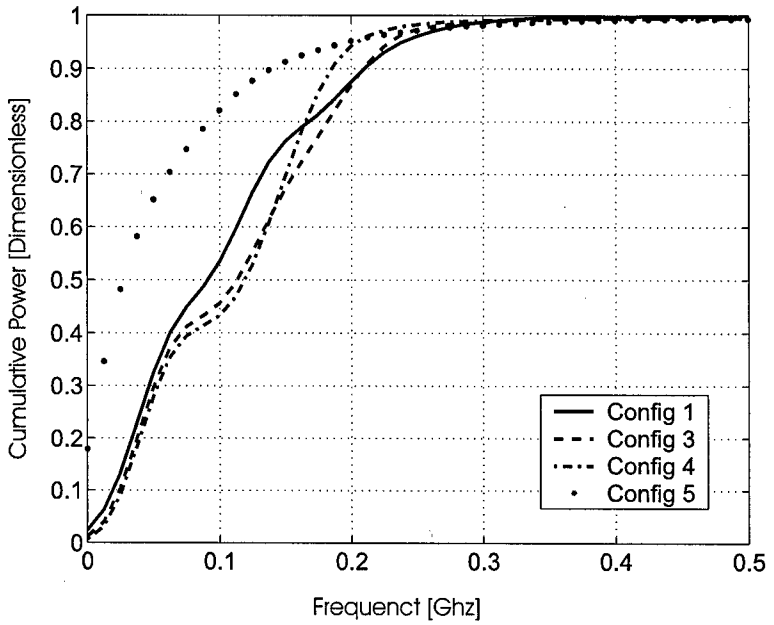


Figure 12: Cumulative energy distribution of the spectra in fig. 10.

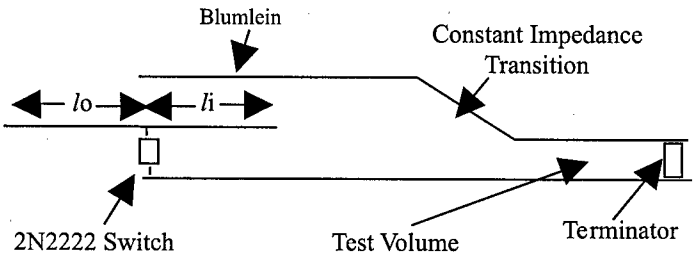


Figure 13: Concept for tuning the center frequency of the pulser.

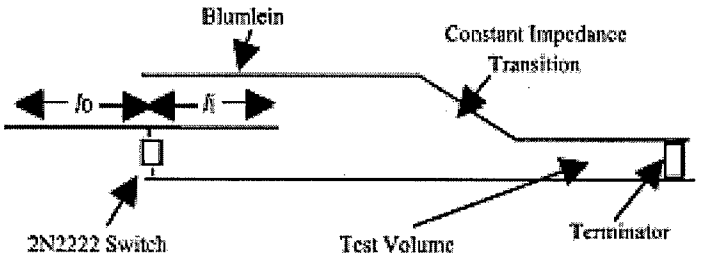


Figure 14: By retracting the center conductor to the positions in table 2, the pulse width can be selected, thereby tuning the center frequency of the Blumlein.

configurations 2 – 5 in table 1.

# 5 High Voltage System Design

## 5.1 HV Switch

We have designed and fabricated a pressurized hydrogen trigatron switch specifically to be integrated into the parallel plate Blumlein geometry. The schematic of the switch assembly cross section is shown in fig. 15. The switch housing was constructed from Ultem 2300 plastic and the electrodes are constructed from CW70E copper tungsten Alloy. The trigger pin is adapted from a modified M&MEW #10-40 model engine spark plug. The switch is shown integrated into the Blumlein in fig. 16 and the entire system is pictured in fig. 17.

## 5.2 Preliminary High Voltage Tests

The trigatron/Blumlein assembly depicted in fig. 16 was pulse charged to 15 kV using an Ultravolt/Behlke power supply with a charge waveform rise time of 50 ns. An EG&G trigger transformer was used to trigger the trigatron. The hydrogen switch was pressurized to 300 psi. The rise time of the switch was on the order of 200 ps, and the shot-to-shot variability of the switch is estimated to be less than 5% (data not shown). Output voltage measurements were made using a capacitive probe connected to a Tektronix SCD 5000 transient digitizing oscilloscope.

Fig. 18 shows the voltage measurements in the output section of fig. 1 for configurations 9 and 10 in table 3. For both of these cases the width of the center conductor was 2.5× larger than the width of the outer conductors. By sliding the center conductor out, the pulse width is decreased as expected. The amplitude of the pulse is somewhat decreased. This effect might be due to the length of the energy storage section ending before the voltage has completely turned on.

Fig. 19 shows the responses for configurations 11 and 12 in table 3. These configurations have the center conductor offset towards the bottom and top conductors, respectively. Comparing the results from fig. 18 and fig. 9, we see that the high voltage system actually appears to have better fidelity in the waveform. This is probably because the trigatron switch depicted in fig. 15

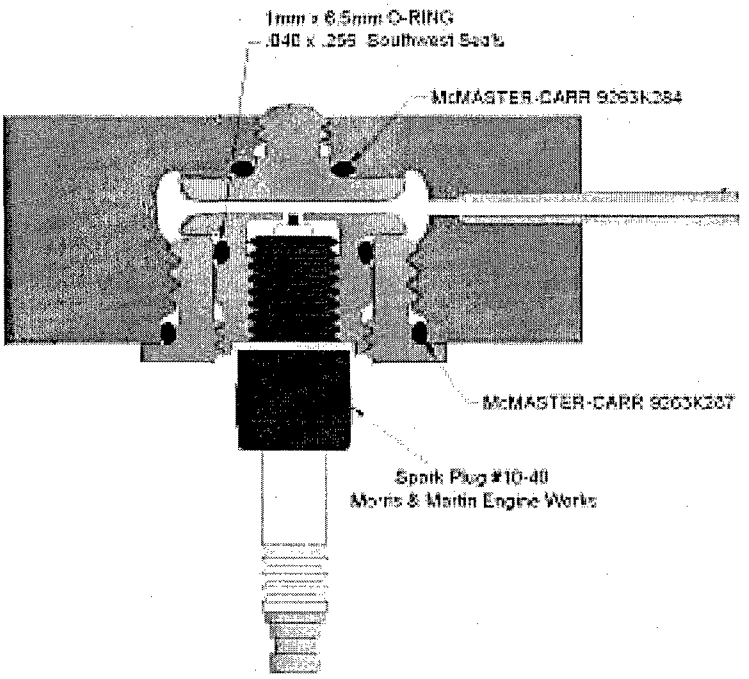


Figure 15: Schematic of the trigatron switch assembly. The overall dimensions are 12.4 mm high by 38.1 mm in diameter.

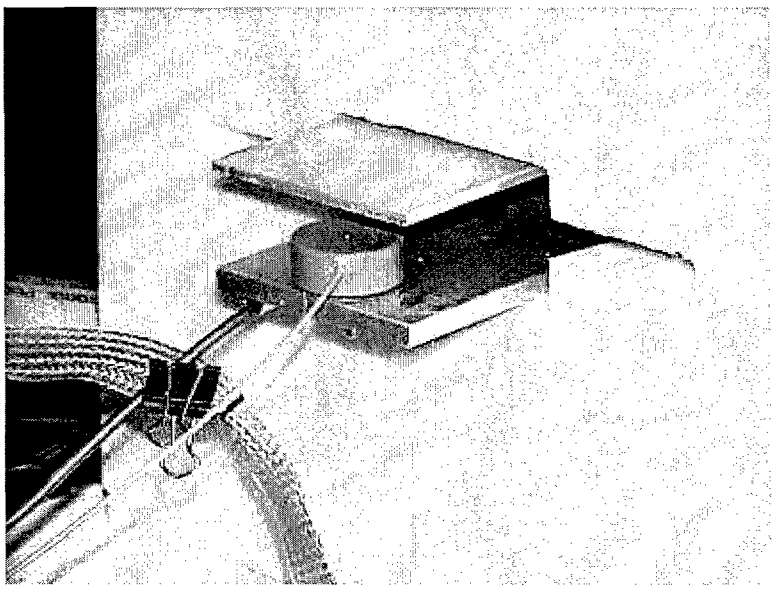

Figure 16: Trigatron switch integrated into the Blumlein test fixture for initial high voltage test.

Table 3: Configurations tested using the high voltage trigatron/Blumlein assembly. The dimensions are referred to fig. 1 and fig. 13. Negative offsets indicate that the center conductor is offset toward the bottom conductor. The top and bottom electrodes were 7.0 cm wide and the total plate separation was 2.9 cm.

| # | $w$ (cm) | offset (mm) | $\ell_i$ (cm) | $\ell_o$ (cm) |
|---|---|---|---|---|
| 9 | 17 | 0 | 30 | 0 |
| 10 | 17 | 0 | 15 | 15 |
| 11 | 7.0 | -7.9 | 30 | 0 |
| 12 | 7.0 | 7.9 | 30 | 0 |

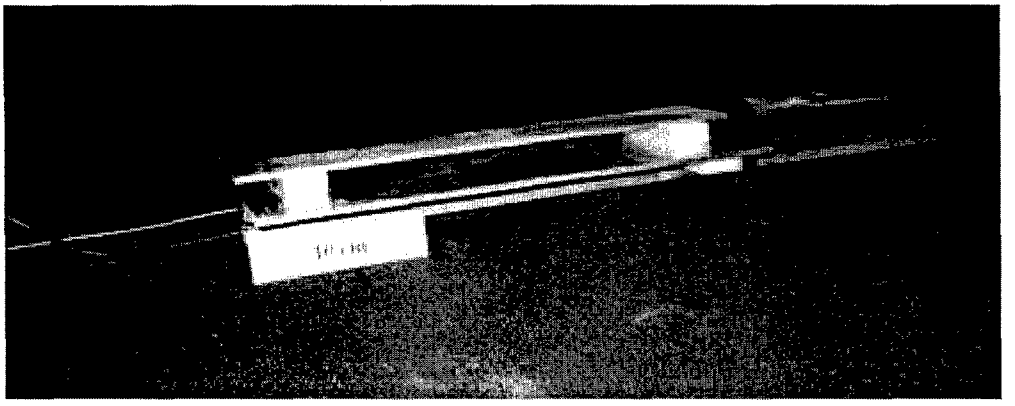

Figure 17: Full system picture of the Blumlein PFN. In this photo, the center electrode is offset towards the bottom electrode (configuration 11). A 10-cm reference is shown.

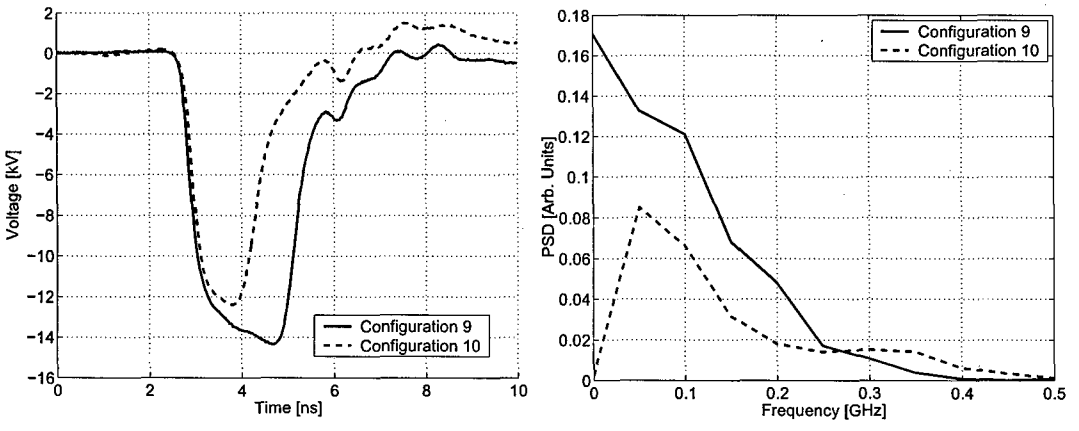


Figure 18: High voltage measurements for configurations 9 and 10 in table 3. The pulse width is narrower for configuration 10 as expected.

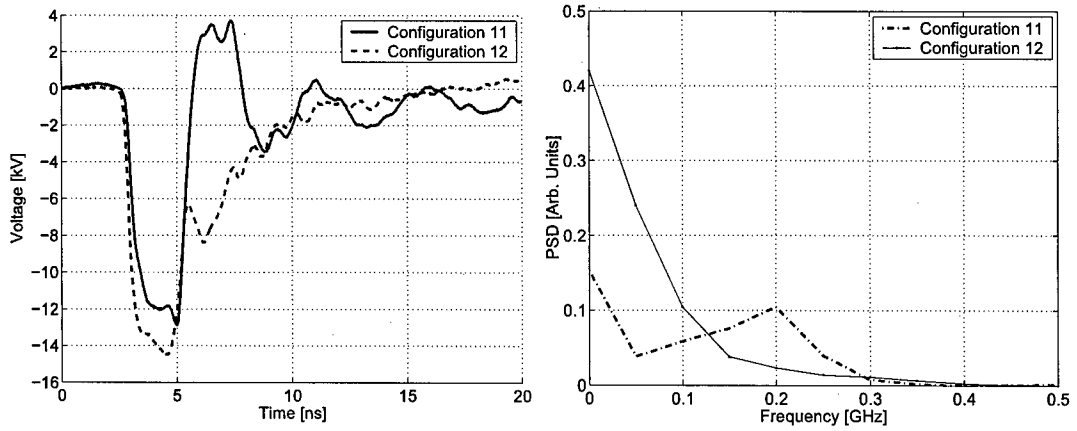


Figure 19: Responses for configurations 11 and 12 in table 3. These two configurations have the center conductor offset towards one of the outer conductors.

was designed specifically to integrate into the parallel plate Blumlein structure, and is a more ideal switch when closed than the 2N2222, with a lower on resistance and less switch inductance.

# 6 Final System Design and Characterization

The prototype systems described in [11] had to be disassembled and reassembled in order to realize the tunability promised by the modeling. A finished system designed to be used in the laboratory should have the ability to be easily reconfigured, and would preferably have fine control over the adjustment parameters. In this section, we describe the mechanical and high voltage design that we used to accomplish these goals.

## 6.1 High Voltage System

The top and bottom conductors were 2.54 cm wide and made from 0.3175-cm-thick sheets of aluminum. The center conductor was made three times wider than the top an bottom conductors to limit parasitic capacitances as discussed above. The center conductor's total length was 33.3 cm, which was the upper limit to the length of the energy storage section.

As is typical for Blumlein pulse forming systems, the center conductor is charged to high voltage with respect to the two exterior conductors. The bottom conductor is held to local ground and the top exterior conductor is resistively tied to the bottom conductor. The center conductor is pulse charged to high voltage using an UltraVolt DC-DC converter. The switch used was a pressurized hydrogen trigatron switch that had been previously designed for integration into this system [11]. The switch was operated at pressures ranging from 100 - 200 psi, and the best performance was found typically around 150 psi. Risetimes on the order of 250 ps were readily obtained with this setup. When the trigatron closes, the combination of impedances between the center and exterior conductors determines the characteristics of the output pulse. The trigatron is triggered using an EG&G TR-180B trigger coil which is driven using a custom trigger system.

The entire system was placed inside an acrylic storage container that was used to contain a bath of sulfur hexafluoride ($SF_6$). The $SF_6$ was necessary in order to prevent flashover from the center conductor to the closer conductor when the center conductor was moved away from the center position.

## 6.2 Mechanical Control

The primary challenges associated with the mechanical design are twofold. First, the remotely controlled positioning equipment needs to be electrically isolated from the high voltage section of the Blumlein. Second, since the outer contuctors are fixed, a slip-contact had to be devised that allows the center conductor to both retract and be displaced without disrupting the functionality of the switch.

### 6.2.1 Control and Actuation

The schematic and photograph of the final mechanical control system is depicted in fig. 20. The system was controlled by a tern programmable computer connected to the system via a fiber optic cable. The computer was used to control the lateral and vertical positions of the center conductor and to fire the high voltage system. The pressure in the hydrogen switch was controlled manually.

## 6.3 Slip-Fitting for the Switch Housing

The current system using the trigatron switch described in [11] has the shortcoming that the rigid switch housing is fixed in size. As the center conductor is offset, the location of the bottom contact moves, and must be compensated for. We addressed this problem using the setup shown in fig. 21. The contact between the switch and the center conductor is made through a pressure contact using a hemispherical copper electrode. The hemispherical electrode is retracted using a solenoid when the center conductor is moved laterally in order to minimize damage to the contacts. The bottom contact of the switch is made to a rigid conductor that has a collar of finger stock. This conductor is fitted into a cylindrical housing that is electrically connected to the bottom conductor.

The design shown in fig. 21 had the problem that the current had to travel down the cylindrical housing, across the finger stock contact, and back up through the switch. As the center conductor was moved vertically, the current path length changed, and the rise time performance of the switch changed (data not shown). Future designs of this section will need to provide electrical contact between the switch and the housing as close to the plane of the bottom conductor as possible. For the purposes of the measurements shown in this paper, this was accomplished using copper tape as a temporary fix.

# 7 System Performance

For the experiments reported here, the system was pulse charged to 25 kV. All measurements were made using a capacitive probe. The data was measured using a Tektronix TDS7440 Digital

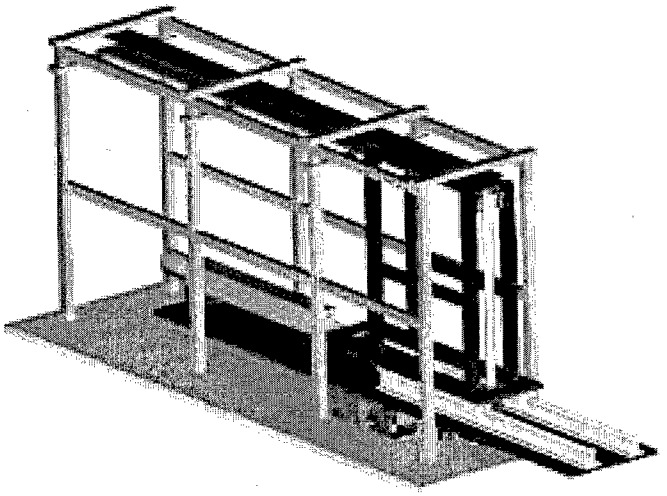

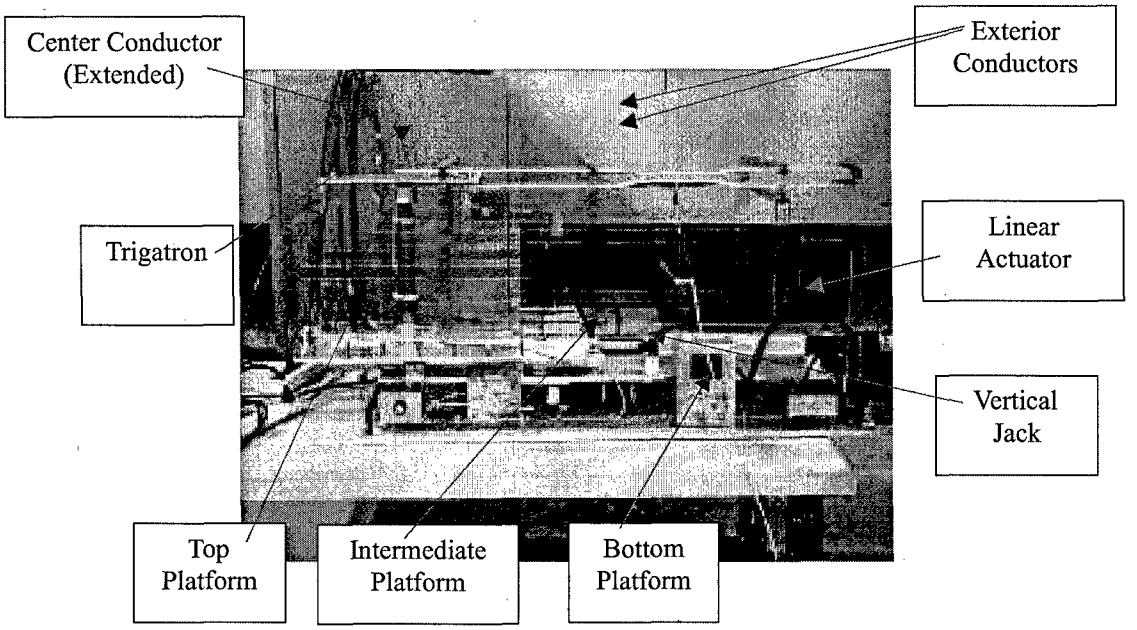


Figure 20: A. Mechanical drawing of the system. The electrical portion of the Blulein is at the top of the drawing, and is coupled to the mechanical actuators at teh bottom via rigid dielectric support posts. B. Photograph of the as-built system.

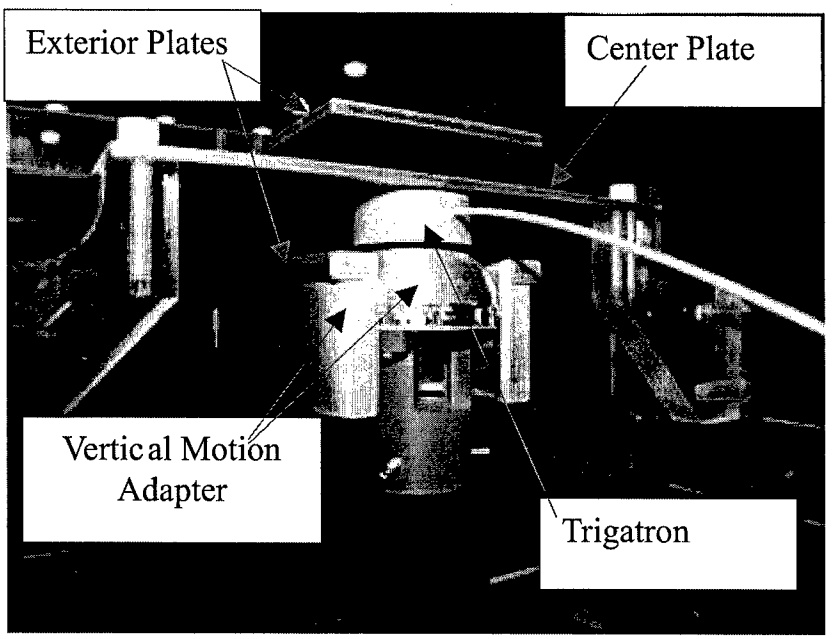


Figure 21: Slip fitting to maintain electrical contact between the switch electrodes and the center and bottom conductors as the Blumlein is tuned.

Sampling Oscilloscope. The system was calibrated and compensated using in-house developed software.

Fig. 22 shows the results of tuning the center frequency by retracting the center conductor at a fixed vertical position. The center electrode was located at 1 mm from the bottom conductor, which produces a 3 - 4 cycle, damped, ringing waveform. The three curves shown in each of the panels were measured with $\ell_i = 333$ [cm] (fully inside the storage region), 253 cm, and 173 cm. The waveforms behave as expected. As the length of the storage region is reduced, the oscillation frequency increases. Fig. 22B shows the Fourier transform of the time domain waveforms. There is a clear shift in the center frequency of the wideband wavefrom to higher frequencies, as is expected from looking at fig. 22A.

In addition to the tuning of the center frequency, the parallel plate Blumlein topology also provides the ability to control the bandwidth of the output waveform for a particular center frequency. Fig. 23 shows the output waveforms of the Blumlein when the center conducter is fully inside the energy storage section for three different vertical positions. The resonant frequency of the system remains stable, but the bandwidth decreases as the center conductor is moved towards the bottom conductor. Since the stored energy is nominally the same in all three cases, the reduction in bandwidth results in a 4 dB increase in the peak power spectral density relative to the case where the center electrode is in the middle of the Blumlein.

Fig. 24 shows similar data obtained when the center conductor was partially retracted from the energy storage region ($\ell_i = 253$ [mm]). As in fig. 23, we see a reduction in bandwidth as the center conductor is shifted towards the bottom conductor. However, the frequency domain data is less consistent than was the case in fig. 23. We believe that this may be due to the effect of

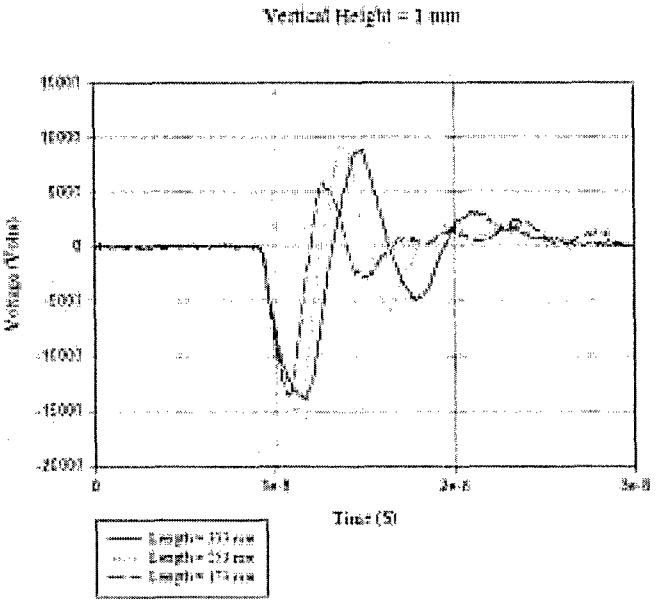


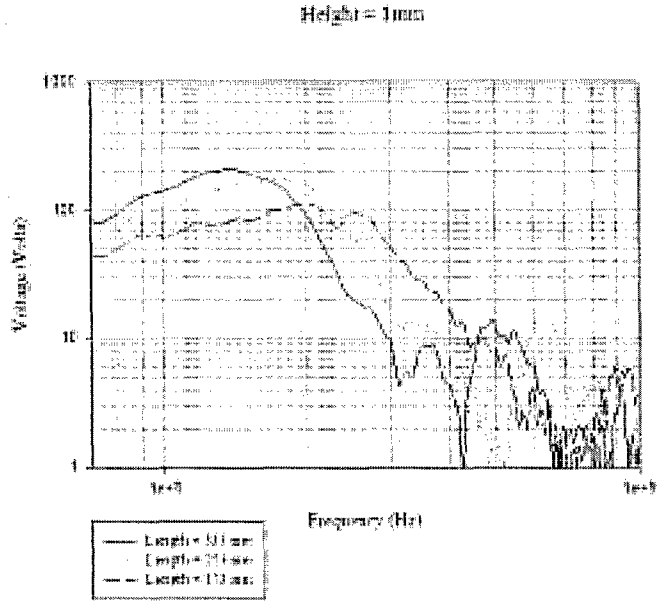


Figure 22: A. Time domain output waveforms for the Blumlein with the center conductor located 1 mm from the bottom conductor with $\ell_i$ = 33.3 cm, 25.3 cm, and 17.3 cm. B. Fourier transforms of the data in panel A.

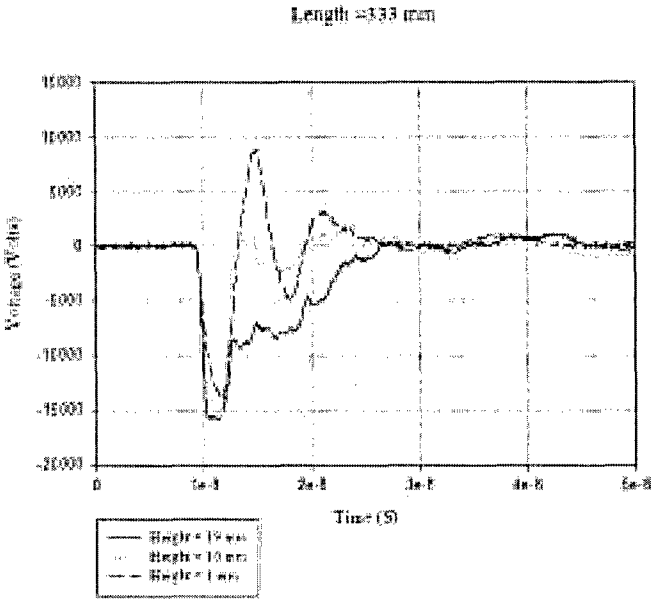


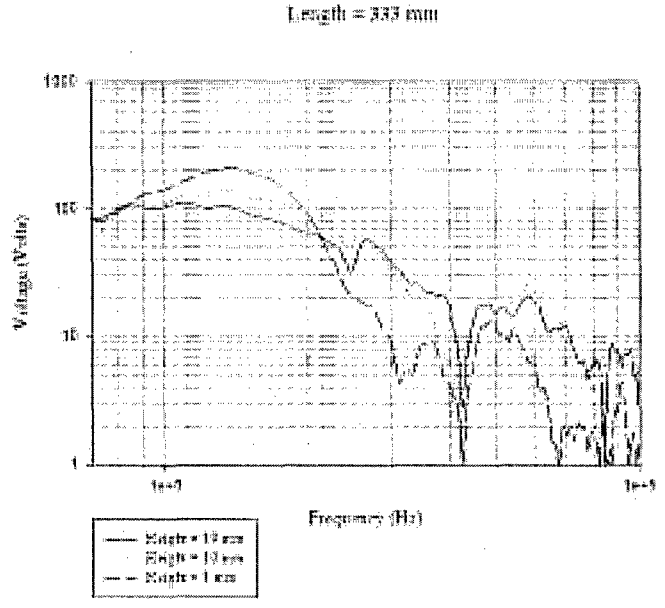


Figure 23: A. Time domain output waveforms for the Blumlein with $\ell_i = 333$ [cm] for the center conductor close to the bottom conductor ($h = 1$ [mm]), centered between the conductors ($h = 10$ [mm]) and close to the top conductor ($h = 19$ [mm]). B. Fourier transforms of the signals in panel A.

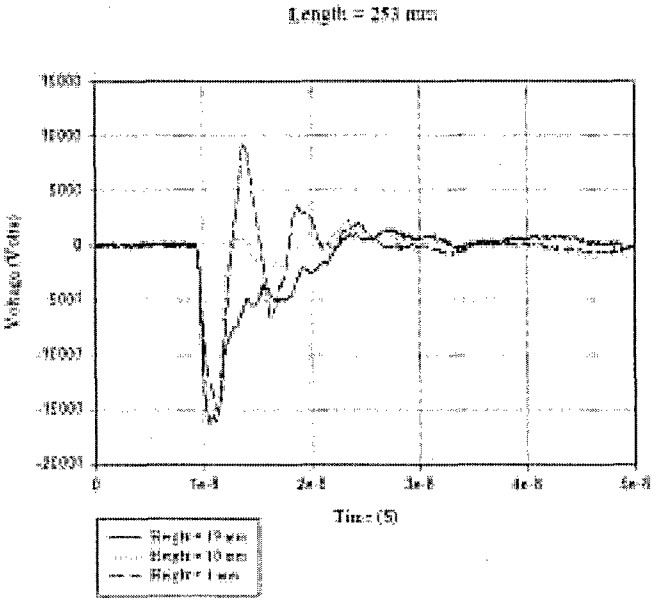


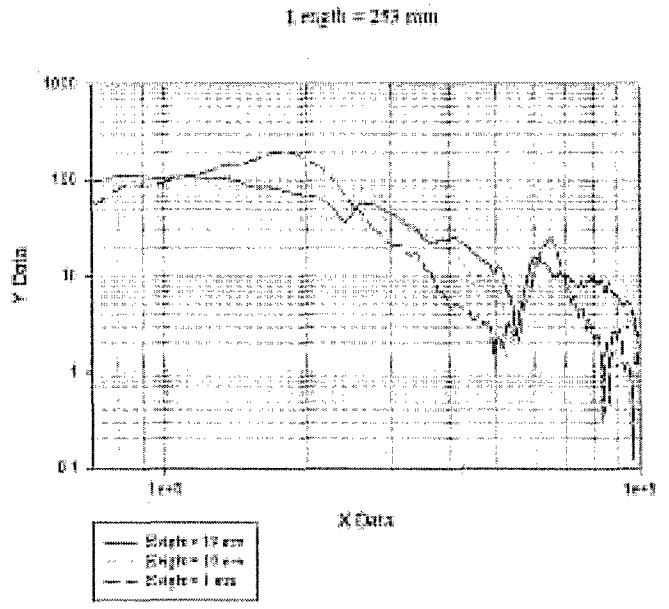


Figure 24: A. Time domain output waveforms for the Blumlein with $\ell_i = 25.3$ [cm] for the center conductor close to the bottom conductor ($h = 1$ [mm]), centered between the conductors ($h = 10$ [mm]) and close to the top conductor ($h = 19$ [mm]). B. Fourier transforms of the signals in panel A.

variable parasitic capacitances at the switch end of the system as the center conductor is retracted. This feature is discussed in greater detail below.

# 8 Discussion

The qualitative performance of the tunable Blumlein system as shown in fig. 22 - fig. 24 was remarkable. However, a quantitative analysis shows that there is still room for improvement in the overall performance of the system.

As was shown in fig. 23 and fig. 24 in section 7 above, the ability of the pulser to maintain a stable frequency as the bandwidth is changed degrades as the center conductor is retracted. In fig. 23, the center frequency is maintained, but in fig. 24, the center frequency shifts significantly towards higher frequnecies when the center conductor is lowered. A possible explanation for this effect is that the portion of the center conductor that sticks out behind the switch as shown in fig. 11 acts as a variable capacitive load. This capacitive load can be thought of as extending the effective length of the Blumlein section. When the center conductor is centered between the top and bottom conductors, both transmission lines see the same capacitive load. However, when the center conductor is shifted, the effective length of the top and bottom transmission lines is slightly different, and this affects the timing of the Blumlein system.

In order to investigate this potential effect, we developed a 2-dimensional electromagnetic simulation using the Partial Differential Equation (PDE) Toolbox (ver. 1.0) in Matlab (ver. 7.0). This simulation was designed to study the additional effective length at the termination of the Blumlein as a function of the plate separation and the amount of the center condutor that is sticking out behind the switch.

The Matlab PDE toolbox is a package that allows the evaluation of the general scalar hyperbolic equation

$$-\nabla \cdot (c\nabla u) + d\frac{\partial^2 u}{\partial t^2} + au = f \tag{5}$$

subjecto to standard boundary conditions that specifiy either the variable $u$ or its normal derivative over a closed computational domain in two dimensions. We assume a two dimensional geometry as shown in fig. 25, and consider only TM fields, so that

$$\mathbf{H} = H_z(x,y)\hat{\mathbf{z}}, \tag{6}$$

and the source free wave equation for $\mathbf{H}$ has the standard form

$$\nabla^2 H_z - \left(\frac{1}{c^2}\right)\frac{\partial^2 H_z}{\partial t^2} = 0 \tag{7}$$

with Neumann boundary conditions

$$\frac{\partial H_z}{\partial n} = 0. \tag{8}$$

The derivative with respect to $n$ in (8) is understood as the normal derivative of the transverse magnetic field. A TEM plane wave with Gaussian temporal behavier (FWHM of 300 ps, corresponding to the rist time of the step in the real experiment). is lauched from the left boundary of

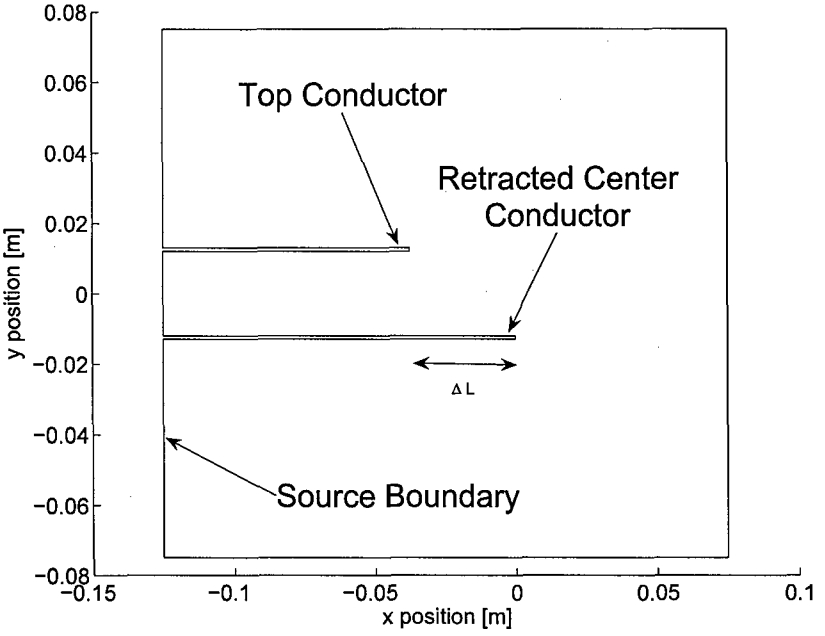


Figure 25: Two-dimensional computational geometry for studying the termination effects of the Blumlein.

the computational domain, and the other three walls were taken as perfect conductors. They were placed far enough away that their effect did not appear until well after the pulse was reflected from the open end of the transmission line.

The current waveform at a position 5 cm from the end of the top conductor is shown in fig. 26 for a number of values of $\Delta L$ in fig. 25. We see in fig. 26 that as the center conductor is retracted, the reflected current waveform arrives later in time. In addition, the reflected current pulse has a lower peak amplitude and a wider pulse width, indicating that some of the high-frequency energy is lost to aperture radiation at the open circuit termination.

We define the additional delay $\Delta t$ of the transmission line to be the additional delay in the reflected current waveform over the case where the center conductor is flush with the outer conductor. We see that the larger gap gives rise to a larger $\Delta t$ for the same $\Delta L$. In the imbalanced Blumlein configuration, this additional delay will cause the timing of the Blumlein to degrade, and the radiation losses will result in a lower $Q$ for the system. These ideas are in agreement with the experimental data in fig. 23 and fig. 24.

# 9 Calculations of vibrations in Biological Samples

Of the various types of molecules found in biological systems, proteins offer the richest set of diversity of vibrational modes that are of interest to us. Other molecules found in biological systems such as lipids, sugars, and nucleic acids also have rich vibrational states, however the function of proteins depend largely on their low frequency vibrational modes we have chosen this

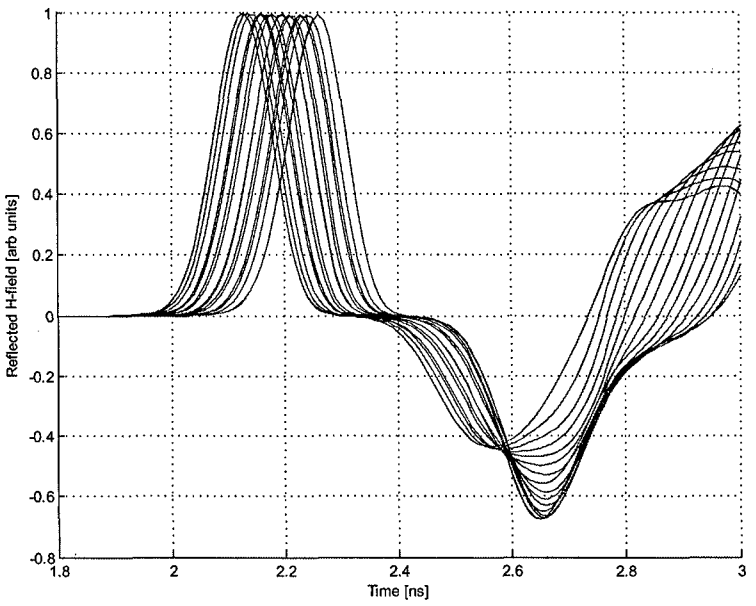


Figure 26: Current waveform as the center plate is retracted from the energy storage section. WE first see the outgoing wave on the line

class of molecules to study.

Much of the difficulty in finding normal modes of proteins is that the force constant matrices are typically poorly conditioned. We are attempting to make a change in basis along the dihedral angels of the peptide chain so that once the matrix is constructed in this alternate basis; the condition number will be small. We hope this will enable us to diagonalize the force constant matrix in a way that will allow us to retrieve the lowest eigenvalues, and their corresponding eigenvectors.

We have found that we cannot rely on most commercial and non-commercial software that we have access to. Typically the packages that are available to find normal modes of molecules are not designed to work with the frequencies that we are interested in. We are attempting to find modes at 3 cm-1 and under. Packages such as Gromacs and Spartan typically do not do well at calculating modes of proteins under 30 cm-1.

We have written code to aid in constructing a model of proteins in both Cartesian space, and "dihedral space". Because the rank of a matrix in "dihedral space" is less than the one in Cartesian space we must fix angles and radii between certain sets of atoms in Cartesian space. Effectively, this process preserves rank and therefore ensures that we can convert from one set of coordinates to the other without losing information, but it comes at a cost that we cannot change any of the internal angles, or make any conformational changes to side chains.

We have written code that can visualize the vibrations when given the eigenvalues of the proteins vibrational mode, as well as the corresponding eigenvector. This will enable us to visually distinguish possible functional roles at differing frequencies. This semester we intend to

complete the "dihedral space" conversion code so that we can import proteins from the RCSB Protein Data Bank (PDB) and represent real proteins with crystal structures that have been reliably determined in our "dihedral space" basis set. Once this is accomplished I hope to test several well understood proteins and see if our program gives reasonable results for the low frequency vibrational modes.

At this point in our work we know how we can find vibrational modes in "dihedral space" using finite difference methods; however this method is unlikely to work well due to numerical error. We are presently working on a method so that we can avoid finite differencing by constructing the force constant matrix in a symbolic form and then substitute numerical values from the crystal structure so that we can find accurate eigenvalues and eigenvectors corresponding to the vibrational modes of the system.

# 10 Conclusions

In this paper we have demonstrated the feasibility of using a parallel plate Blumlein architecture to create a pulser with tunable output characteristics. The strategy relies on the parasitic impedances and the imbalance in impedance that occurs by moving the center conductor in the parallel plate Blumlein architecture. The methods used here are best suited for use with high impedance Blumleins – lower impedance structures have lower parasitic capacitance and much tighter tolerances for tuning. In addition to tuning the $Q$ of the PFN, the center frequency can be simply modified by sliding the center conductor out of the PFN section. We have demonstrated the feasibility of this strategy through the use of electromagnetic and circuit simulations, as well as through a series of low voltage tests.

In addition to the demonstration of the strategy, we have also presented preliminary designs for some of the key aspects of the high voltage version of the system. The compact hydrogen switch described in section 5.1 has a rise time of less than 200 ps at a charge voltage of 15 kV when integrated into the test fixture. Initial high voltage measurements with the new switch and the offset center conductors have demonstrated the consistency of the results seen in the low voltage tests. We are currently working on the final design of the high voltage system to allow for continuous tuning of both center frequency and bandwidth. In addition to tuning the parameters discussed in this paper, we are working on methods to tune the amplitude and rise time of the waveforms for additional flexibility. The resulting tunable pulser will be well suited for use in studying the wideband electromagnetic interaction with electrical and biological systems.

# 11 Personnel Supported

The following personnel were either supported on DEPSCoR funds (either Federal or Cost Share) during the period covered by this report or were associated with the project.

Associate Professor J. Scott Tyo, ECE Department, UNM
Associate Professor Deborah G. Evans, Chemistry Department, UNM
Mr. Jinhui Chen, Graduate Student, ECE Department, UNM (Graduated, MS, 2004)

Mr. Mark Fleharty, Graduate Student, Computer Science Department, UNM
Mr. Mustafa Dogan, Graduate Student, ECE Department, UNM (Graduated, MS, 2005)
Mr. James Boddeker, Undergraduate/Graduate Student, ECE Department, UNM
Mr. Michael C. Skipper, Senior Engineer, ASR Corporation
Mr. Michael D. Abdalla, Senior Engineer, ASR Corporation
Mr. Samuel Romero, Engineering Technician, ASR Corporation
Mr. Brett Cockreham, Senior Mechanical Engineer, Solid Design, Inc.

# 12 Publications and Presentations Associated with DEPSCoR

## 12.1 Journal Articles

1. J. S. Tyo, M. C. Skipper, M. D. Abdalla, S. P. Romero, and B. Cockreham, "Frequency and Bandwidth Tunable Pulser for Use in Wideband Applications," *IEEE Trans. Plasma Sci.*, **32**:1926 – 1931 (2004)

2. J. S. Tyo, E. G. Farr, J. S. H. Schoenberg, L. H. Bowen, and L. L. Altgilbers, "Time and Frequency domain radiation patterns of reflector impulse radiating antennas: effect of aperture field distributions," *IEEE Trans. Antennas Propagat*, **52**: 1767-1776 (2004)

3. J. Gaudet, R. J. Barker, M. Gunderson, A. Kuthi, A. Neuber, J. Dickens, W. Nunnaly, E. Schamiloglu, C. Christodoulou, J. S. Tyo, K. Schoenbach, R. Joshi, M. Laroussi, J. Kolb, and R. Vidamr, "Research Issues in Developing Compact Pulsed Power for High Peak Power Applications on Mobile Platforms," *Proc. IEEE*, **92**:1144 – 1165 (2004)

4. M. J. Baretela and J. S. Tyo, "Improvement of Prompt Radiated Response from Impulse Radiating Antennas by Aperture Trimming," *IEEE Trans. Antennas Propagat.* **51**:2158 – 2167 (2003)

## 12.2 Conference Proceedings

1. J. Chen, C. J. Buchenauer, and J. S. Tyo, "Modeling the conductivity of a subnanosecond breakdown gas switch," submitted to *Ultra Wideband, Short Pulse Electromagnetics 7*, F. Sabath and E. Mokole, Eds., (Plenum, NY, In Press)

2. J. S. Tyo, "Aperture Engineering for Impulse Radiating Antennas," submitted to *Ultra Wideband, Short Pulse Electromagnetics 7*, F. Sabath and E. Mokole, Eds., (Plenum, NY, In Press)

## 12.3 Conference Presentations

1. J. S. Tyo, C. J. Buchenauer, and J. Boddeker, "Improvement of aperture efficiency in impulse radiating antennas by polarization control," *2004 IEEE Antennas and Propagation International Symposium*, Monterey, CA, June

2. B. Minhas, J. S. Tyo, K. J. Malloy, S. R. Brueck, "Some comments on perfect imaging in materials with negative permittivity and permeability," *2004 URSI Commission B Electromagnetic Theory Symposium*, Pisa, Italy, May

3. J. S. Tyo, C. J. Buchenauer, E. G. Farr, and L. H. Bowen, "Theory and measurements of defocused impulse radiating antennas," *PIERS 2003*, Waikiki, HI, October 13 – 16

### 12.4 Conferences Attended

1. PIERS 2003, Honolulu, HI, October
2. American Physical Society Annual Meeting, Albuquerque, NM, November
3. 2004 URSI Commission B International Electromagnetic Theory Symposium, Pisa, Italy, May
4. 2004 IEEE Antennas and Propagation International Symposium, Monterey, CA, June
5. EUROEM 2004, Magdeburg, Germany, July

## 13 Honors and Awards

1. J. S. Tyo was awarded the Ultra-Wideband, Short PUlse 7 Best Paper Award, EUROEM 2004, Magdeburg, Germany

## References


[1] W. D. Prather, C. E. Baum, J. M. Lehr, J. P. O'Laughlin, J. S. Tyo, J. S. H. Schoenberg, R. J. Torres, T. C. Tran, D. W. Scholfield, J. Gaudet, and J. W. Burger, "Ultra-wideband source and antenna research," *IEEE Trans. Plasma Sci.*, vol. 28, pp. 1624–1630, 2000.

[2] D. V. Giri and C. E. Baum, "Temporal and spectral radiation on boreight of a reflector type of impulse radiating antenna (IRA)," in *Ultra-Wideband, Short-Pulse Electromagnetics 3* (C. E. Baum, L. Carin, and A. P. Stone, eds.), pp. 65–72, New York: Plenum, 1997.

[3] D. V. Giri, W. L. Baker, W. D. Prather, J. M. Lehr, D. V. Giri, J. P. O'Laughlin, I. D. Smith, R. Altes, J. Fockler, D. P. McLemore, M. D. Abdalla, and M. C. Skipper, "Jolt: a highly directive, very intensive, impulse-like radiator," *Proc. IEEE*, vol. 92, pp. 1096 – 1109, July 2004.

[4] C. E. Baum, "From the electromagnetic pulse to high-power electromagnetics," *Proceedings of the IEEE*, vol. 80, pp. 789 – 817, 1992.

[5] K. H. Schoenbach, S. Katsuki, R. H. Stark, E. S. Buescher, and S. J. Beebe, "Bioelectrics-new applications for pulsed power technology," *IEEE Trans. Plasma Sci.*, vol. 30, pp. 293–300, 2002.

[6] F. Davanloo, C. B. Collins, and F. J. Agee, "High-power, repetitive-stacked blumlein pulsers commutated by a single switching element," *IEEE Trans. Plasma Sci.*, vol. 26, pp. 1463 – 1475, 1998.

[7] J. S. H. Schoenberg, J. W. Burger, J. S. Tyo, M. D. Abdalla, M. C. Skipper, and W. R. Buchwald, "Ultra-wideband source using gallium arsenide photoconductive semiconductor switches," *IEEE Trans. Plasma Sci.*, vol. 25, pp. 327 – 334, 1997.

[8] Integrated Engineering Software Sales Inc., 220-1821 Wellington Avenue, Winnipeg, Manitoba, Canada R3H 0G4, *Electro 6.1.*

[9] R. E. Collin, *Field Theory of Guided Waves, Second Edition.* New York: IEEE Press, 1991.

[10] Cadence Design Systems, Inc., 555 River Oaks Parkway, San Jose, CA, 95134, *PSpice 9.1.*

[11] J. S. Tyo, M. C. Skipper, M. D. Abdalla, S. P. Romero, and B. 'Cockreham, "Frequency and bandwidth agile pulser for use in wideband applications," *IEEE Trans. Plasma Sci.*, vol. 32, pp. 1925 – 1931, October 2004.